

TIME-OF-FLIGHT ESTIMATION IN ACOUSTIC PYROMETRY: SENSITIVITY TO PULSE CHARACTERISTICS

Matteo Pettinari
University of Pisa (DESTeC)
Largo Lucio Lazzarino, 1
56122 – Pisa – Italy
matteo.pettinari@phd.unipi.it

Lorenzo Ferrari
University of Pisa (DESTeC)
Largo Lucio Lazzarino, 1
56122 – Pisa – Italy
lorenzo.ferrari@unipi.it

ABSTRACT

Acoustic pyrometry is a non-intrusive measurement technique that may have several applications in turbomachinery. This methodology estimates the gas temperature by measuring the time of flight of an acoustic wave moving through a medium. It can be accomplished by placing a sound source (emitter) and a set of microphones (receivers) on opposite sides of a section. The emitter generates a sound pulse, and the receivers detect it. Since the emitter-receiver distances are known and fixed, the average temperatures of the paths traversed by the acoustic pulse can be computed by estimating the time-of-flight through deconvolution techniques. However, despite the straightforward principle, an acoustic wave suffers a variation of amplitude when propagating within a medium because of energy losses and ambient noise. Hence, time-of-flight estimation becomes a critical task, especially when considering high-frequency waves or short distances between sensors. It is then fundamental to select proper acoustic waves to maximise the cross-correlation between the signals of the emitter-receiver couples, thus improving the accuracy of the time-of-flight measurements and, consequently, the estimation of the spatial temperature distribution within a specific area. This study is a preliminary investigation, based on a modelling approach, to estimate the impact of different acoustic waves on the accuracy of the time-of-flight measurement. The results of this analysis will be useful to design and setup an acoustic pyrometry application.

NOMENCLATURE

Abbreviations:

AP acoustic pyrometry
ERC emitter-receiver couple

Symbols:

TOF time-of-flight (s)
T temperature (K)
p pressure (Pa)
f frequency (Hz)

RH relative humidity (%)
SPL sound pressure level (dB)
SNR signal-to-noise-ratio (dB)
B bias (Pa)
SF scaling factor (-)
RE relative error (%)

Superscripts and subscript:

0 reference state
exh exhaust
act actual
est estimated
s sampling

1. INTRODUCTION

Gas temperature is a fundamental parameter in industrial systems' operations as it can be used for performance estimation, operating point control, and diagnostic purposes.

Several methods are typically used to measure the gas temperature. They are mainly organised into two categories: intrusive and non-intrusive techniques. Intrusive techniques are the most conventional ones and rely on arrays of physical probes (i.e., thermocouples, thermistors) adequately placed within a control section to measure local temperature values. Despite their ease of use, these techniques require sensors to be exposed to the operating fluid, thus offering an overall lower maximum temperature of use and a limited resistance in a hostile environment [1]. Moreover, probes directly interact with the gas, potentially altering its local physical properties and causing unintentional errors. Furthermore, devices such as thermocouples require thermal equilibrium with the medium, thus presenting limitations in case dynamic measurements are needed.

Non-intrusive techniques constitute the second category. Conversely to the invasive one, contactless methods allow for remote temperature measurement, thus avoiding the abovementioned drawbacks. Among these techniques, acoustic pyrometry (AP) is gaining more and more interest in turbomachinery due to its multiple advantages, such

as limited intrusiveness, relatively simple set-up, and nearly instantaneous measurements, which makes this method particularly suited for control and real-time applications. Nowadays, its operating principle is well-known as it exploits the compressible flow relationship between the speed of an isentropic sound wave propagating within a gas and its internal temperature. In particular, the methodology measures the gas temperature by estimating the time-of-flight (TOF) of an acoustic wave moving within a medium through deconvolution techniques [1]. Typically, it can be done by placing a sound source (emitter) and a set of microphones (receivers) on opposite sides of a section. The emitter generates a sound pulse at a given instant, and the receivers detect it. Since the emitter-receiver distances are known and fixed, the average speed of sound of the paths traversed by the acoustic pulse can be computed. Consequently, the temperature distribution of the section can be estimated.

Several industrial applications using acoustic pyrometry have been reported in the literature. For instance, acoustic pyrometry proved to be a valuable tool for measuring gas temperatures in the furnace and superheater regions in boilers. Bramanti et al. [2] presented two classes of reconstruction algorithms based on AP to measure an industrial boiler's temperature distribution. Despite the small data set, they showed a fair match between simulated and experimental results, underlying how the technique's resolution depends on the number of available TOF data, thus, on the number of ERCs. Furthermore, Kong et al. [3] used AP to reconstruct the 3D temperature field in an electric heating furnace. They also considered the refraction effect of sound waves in their proposed algorithm.

Concerning the turbomachinery field, Kleppe et al. [4,5] investigated the use of AP for analysing gas temperature and velocity within a single combustor of gas turbine and jet engines. They pointed out how,

conversely to traditional methods, the technique is suitable for control as it does not suffer thermal lag. DeSilva et al. [6,7] successfully used the method to measure a heavy-duty gas turbine's exhaust gas temperature distribution. In their investigation, they underlined how the turbomachinery's flow velocity, mass flow and turbulence levels require alternative sound signals conversely to high-intensity pulses typically used in furnaces and boilers. Furthermore, at the end of their experiment, they concluded that the chirp signal was the most robust to calculate the TOF in noisy environments. More recently, Otero et al. [8] used AP to simultaneously measure jet velocity and static temperature fields in subsonic flows. In the study, they conducted a sensitivity analysis to assess the influence of different parameters on the accuracy of the reconstruction technique. The results suggested how both the size of the devices used in the computational procedure and the emitter-receiver couple (ERC) number significantly affect the estimation accuracy and the computational burden. The reliability of the acoustic pyrometry with respect to the number of ERCs used and TOF uncertainty was further investigated by Ferrari et al. [9–11] through a statistical approach. As a general result, they found that if the TOF estimation is not affected by uncertainty, the estimation accuracy may be improved simply by increasing the number of ERCs. Conversely, if the TOF estimation is affected by some inaccuracies, then an optimal configuration exists to minimise the temperature map reconstruction error.

From a general standpoint, several aspects may influence the quality of gas temperature reconstruction via AP. For instance, factors such as the modelling assumptions, reconstruction algorithm, ambient noise, and the pyrometer set-up may introduce uncertainty in the TOF measurements. Furthermore, the type of signal used may affect the TOF estimation, thus yielding poor temperature estimations. In this context, this study

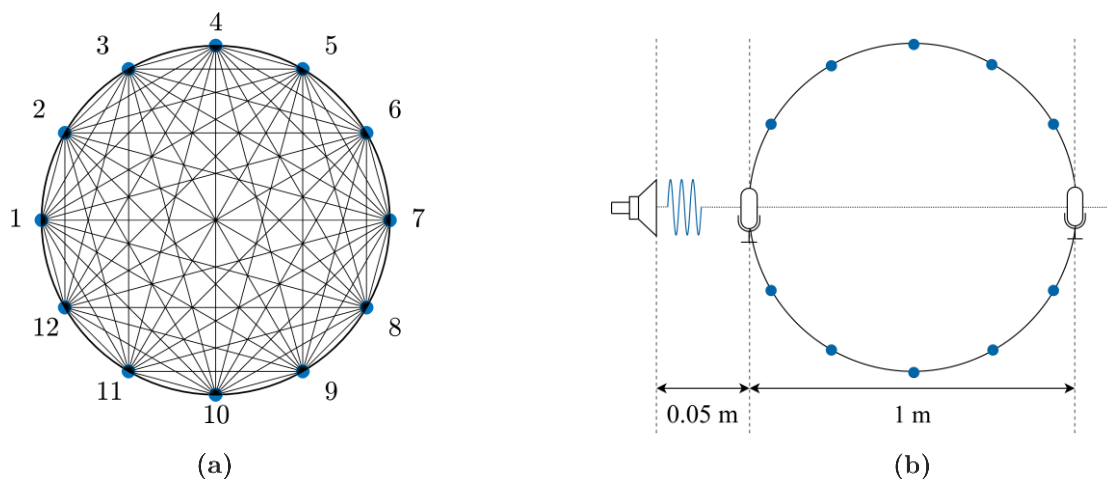


FIGURE 1: ACOUSTIC PYROMETER SET-UP: (a) ERCs DISPOSITION; (b) ERC SIMPLIFIED SCHEMATIC

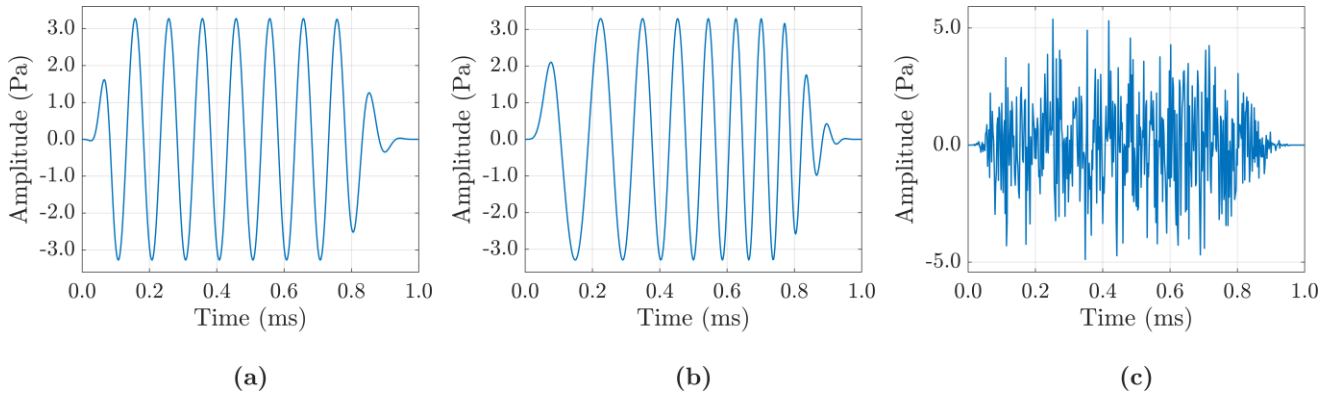


FIGURE 2: TEST SIGNALS: (a) PURE TONE; (b) LINEAR CHIRP; (c) WHITE NOISE

investigates the impact of different acoustic waves on the accuracy of the TOF measurement for given boundary conditions, such as the test signal intensity, ambient noise level, atmospheric attenuation, and sampling capability of the hardware. Therefore, despite being a preliminary study, the study aims at providing valuable guidelines for setting up an acoustic pyrometry application.

2. MATERIALS AND METHODS

2.1 Case study

In this study, an acoustic pyrometer similar to the one proposed by DeSilva et al. [7,8] was considered. Therefore, heavy-duty gas turbine exhaust was assumed to flow inside a stainless-steel pipe with a diameter of 1 m. The temperature and pressure of the turbine exhaust were supposed to be $T_{\text{exh}} = 813.15$ K and $p_{\text{exh}} = 101325$ Pa, respectively, whilst the gas relative humidity was considered $RH = 70\%$. With reference to Figure 1a, several ERCs were assumed to be installed at opposite sides of the pipe, thus determining a sensible area orthogonal to the exhaust flow. Here, the exhaust flow velocity (~ 180 m/s) was assumed negligible compared to the speed of sound (~ 560 m/s). As shown in Figure 1b, each emitter-receiver couple was supposed to comprise a speaker (i.e., pneumatic or electrodynamic speaker) and a pair of microphones. The transmitter operating principle was assumed to be straightforward: at a given instant, the speaker generates a high-intensity acoustic signal that is consequently measured by the pair of microphones. Therefore, the time between detecting the two signals constitutes an estimate of the TOF.

2.2 Synthesis of the signals

In this analysis, three acoustic signals were considered: a 10 kHz pure tone, a linear chirp from 4 kHz to 18 kHz, and white noise.

Due to the short acoustic path length (i.e., the distance between the microphones) and the high sound speed related to the exhaust temperature, the

signals' duration was set at 1 ms. A 0.1 ms and 0.25 ms fading was then applied to simulate the firing and shut-off of the signal emissions, respectively. Signals were assumed to be sampled with a sampling frequency in the 0.05–1MHz range, and their amplitudes were selected to guarantee a predetermined sound pressure level (SPL) in the 80–120 dB range. The SPL definition is provided in the Eq. 1 for the sake of clarity:

$$SPL = 20 \log_{10} \left(\frac{P}{P_0} \right) \quad (1)$$

where P is the signal's root mean square of sound pressure and $P_0 = 20 \mu\text{Pa}$. Figure 2 reports the time-domain representation of test signals of $SPL = 100$ dB sampled at 500 kHz.

To account for the energy losses due to propagation within the gas medium, each test signal was attenuated according to the sound atmospheric attenuation proposed by Burnside [12]. Figure 3 shows the absorption coefficients for the given exhaust conditions, geometrical set-up (i.e., speaker-outer microphone distance), and varying signal frequencies. Each absorption coefficient was applied to the corresponding frequency content of

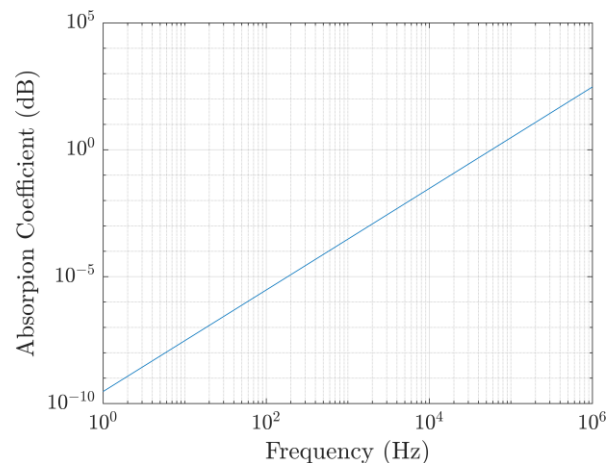


FIGURE 3: ATMOSPHERIC ATTENUATION COEFFICIENTS ($T=540^\circ\text{C}$, $p=101325$ Pa, $RH=70\%$, $L=1.0$ 5m)

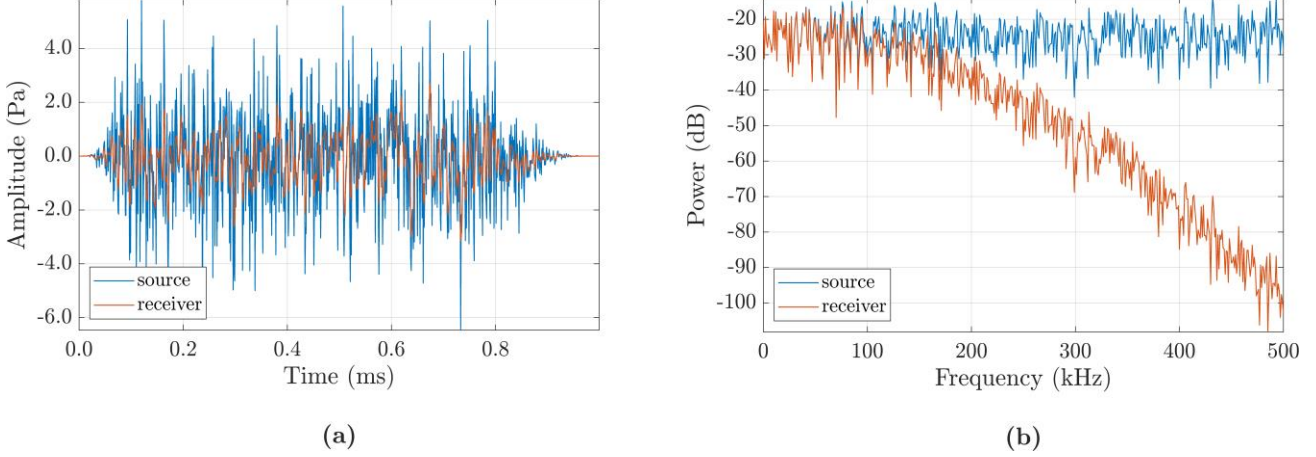


FIGURE 4: WHITE NOISE BEFORE AND AFTER SOUND ATTENUATION: (a) TIME DOMAIN REPRESENTATION; (b) POWER SPECTRUM

the signal power spectrum. It is worth noting that the higher the frequency, the higher the attenuation. Therefore, it is essential to consider sound attenuation, especially when broadband signals such as white noise are considered. Figure 4 reports the time-domain representation and the power spectrum of the test signal shown in Figure 2c, before and after the sound attenuation. It can be noted that the atmospheric attenuation damps the higher frequencies, thus operating as a low pass filter.

Each attenuated signal was then shifted in time to simulate the different detection at the receivers. A constant speed of sound along a straight acoustic path was assumed to compute the travel times from the speaker to the microphone pair. White Gaussian noise was added to account for the ambient noise due to the gas turbine operation. Different, uncorrelated noise series having the same SPLs were used at the two receivers. Finally, microphones' non-idealities were considered by employing the sensor model described as follows:

$$\begin{bmatrix} y_1 \\ y_2 \end{bmatrix} = \begin{bmatrix} B_1 \\ B_2 \end{bmatrix} + \begin{bmatrix} SF_1 & 0 \\ 0 & SF_2 \end{bmatrix} \begin{bmatrix} x_1 \\ x_2 \end{bmatrix} + \begin{bmatrix} w_1 \\ w_2 \end{bmatrix} \quad (2)$$

where x_i , y_i represents the shifted and measured signals, whilst B_i , SF_i , and w_i represent the sensors' biases, scaling factors and noise measurement, respectively. The measurement noise was assumed to be white Gaussian noise with negligible SPL. Therefore, it was supposed to be embedded in the ambient one. Figure 5 reports an example of an artificial chirp signal processed by the ERC couple according to the procedure previously described.

2.3 Estimation error

A TOF estimate was obtained by cross-correlating the signals ideally measured by the pair of microphones. Figure 6 reports an example of normalised correlation coefficients for each considered test signal. The relative error between the

actual (computed) and estimated TOF was then used to assess the goodness of the estimate:

$$RE = 100 \frac{|TOF_{act} - TOF_{est}|}{TOF_{act}} \quad (3)$$

where the subscripts *act*, *est* denote the actual and estimated value, respectively.

2.4 Sensitivity analysis

A sensitivity analysis was performed to investigate which test signals were most suitable for AP applications. To this extent, the scenario depicted in Section 2.1 was considered, and the exhaust conditions were kept constant throughout the analysis. White Gaussian noise of SPL = 100 dB was assumed as ambient noise caused by the gas turbine operation. Table 1 reports the sensors' parameters characterising the pair of microphones.

TABLE 1: SENSOR MODEL PARAMETERS

Parameter	Value	Unit Measure
B_1	0.7	Pa
B_2	-0.5	Pa
SF_1	1.01	-
SF_2	0.97	-

A 19×6 test matrix was then considered. Each matrix element (i.e., configuration) represents a pair of sampling frequency in the 0.05–1 MHz range and signal sound pressure level in 80–105 dB. The sampling frequency range was discretised employing a varying discretisation step, whilst the SPL range was discretised with a constant step of 5 dB. Hence, 114 configurations were obtained.

For each acoustic wave and configuration, the procedure described in Section 2.2 was used to generate artificial measured signals at the two receivers. Signals were then compared via cross-correlation, and the delays corresponding to the maximum normalised correlation values were taken

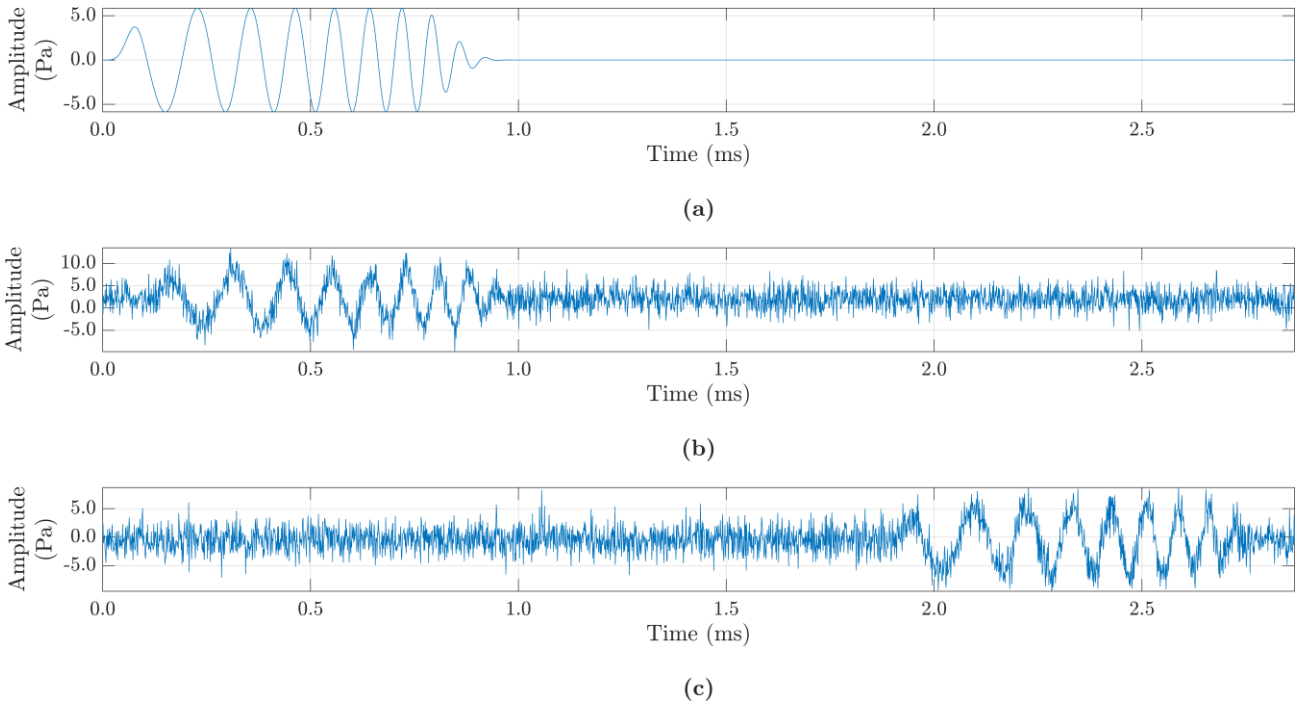


FIGURE 5: EXAMPLE OF LINEAR CHIRP SYNTHESIS: (a) SPEAKER; (b) FIST MICROPHONE; (c) SECOND MICROPHONE

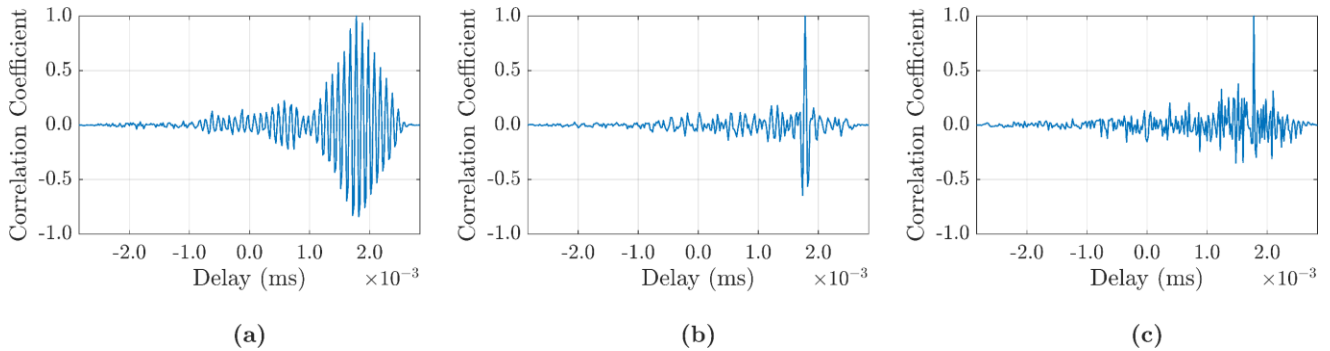


FIGURE 6: NORMALIZED CORRELATION COEFFICIENT: (a) PURE TONE; (b) LINEAR CHIRP; (c) WHITE NOISE

as TOF estimates. Finally, estimation errors were computed according to Eq. 3 and used to generate error maps through interpolation techniques.

3. RESULTS AND DISCUSSION

Figure 7 reports the outcome of a single test run performed for each test signal, assuming the scenario described in Section 2.4. As shown in Figure 7c, white noise yields an estimation error of less than 1% as long as the signal SPL is greater or equal to the ambient noise (i.e., $SPL \geq 100$ dB). On the other hand, when low-intensity white noise is considered (i.e., $SPL < 100$ dB), elevated errors are obtained. Therefore, to be properly detected, white noise must be more intense than ambient noise. In other terms, a favourable signal-to-noise ratio SNR is required to guarantee acceptable TOF estimates, regardless of the sampling frequency.

Different results were obtained when considering the pure tone and linear chirp test

signals, as reported in Figure 7a and Figure 7b, respectively. Contrarily to the white noise, the usage of higher sampling frequencies allows for minor estimation errors even if test signals with SPL lower than the ambient noise one are used. This is because the pure tone and linear chirp have energy concentrated in narrow frequency bands. Thus, their correlation is affected only by the noise contributions at those frequencies.

It is worth noting that the results presented in Figure 7 derive from a single realisation of ambient noise. Therefore, different results could be obtained depending on the time at which the measurement occurs. To better investigate the influence of the ambient noise relative to the TOF estimation error, 1000 test runs were conducted. Also in this case, the conditions outlined in Section 2.4 were considered. For each test matrix configuration, the estimation

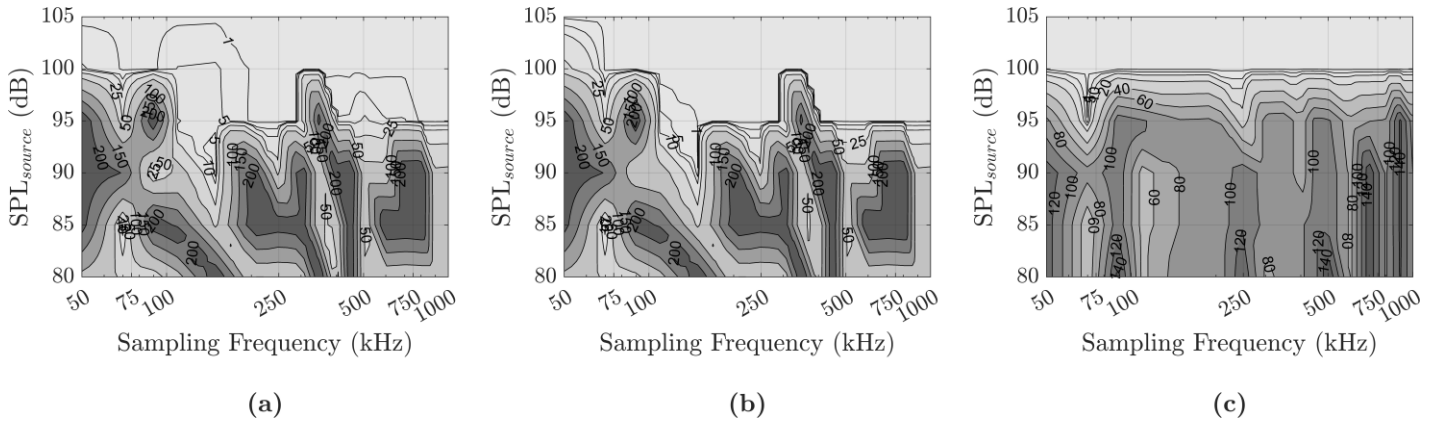


FIGURE 7: TOF ESTIMATION ERROR MAPS ($SPL_{noise}=100$ dB; $N_{tries}=1$): (a) PURE TONE; (b) LINEAR CHIRP; (c) WHITE NOISE

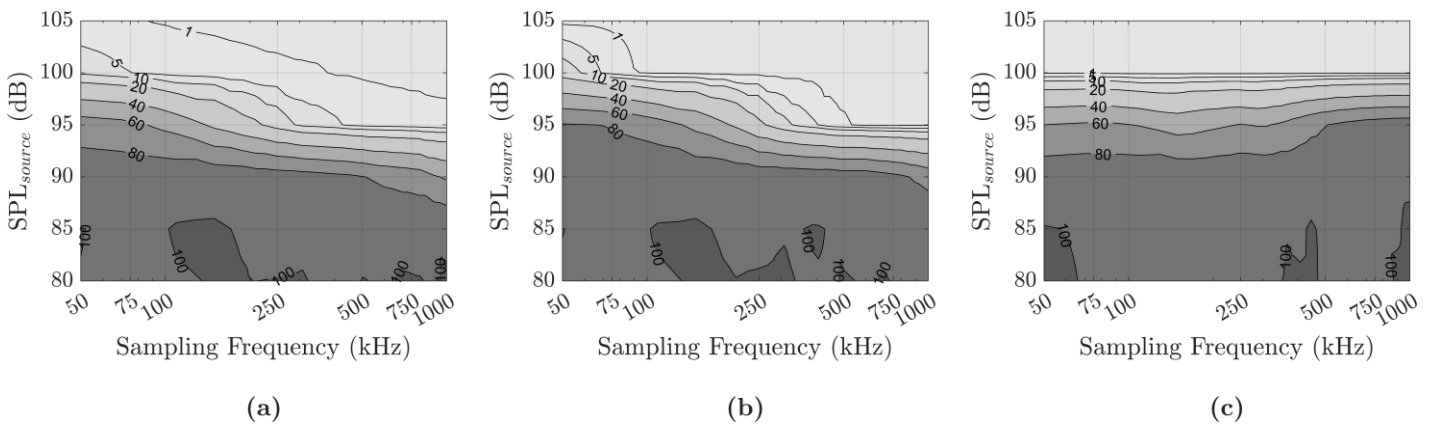


FIGURE 8: TOF ESTIMATION AVERAGE ERROR MAPS ($SPL_{noise}=100$ dB; $N_{tries}=1000$): (a) PURE TONE; (b) LINEAR CHIRP; (c) WHITE NOISE

errors were averaged. The averaged errors were then used to generate the distribution error maps.

Figure 8 reports the average TOF error maps generated through the 1000 trials. With reference to Figure 8c, it can be observed that the white noise presents almost constant error curves depending on the signal SPL. Higher sampling frequencies also seem to worsen the TOF estimates when low SNR values are considered. On the other hand, pure tone and linear chirp yield decreasing TOF estimation error curves for a given SPL and an increasing sampling frequency, as reported in Figure 8a and Figure 8b. Despite the similar error trend, linear chirp proves to be more robust when compared to the pure tone. For instance, linear chirp returns estimation errors lesser than 1% already at medium sampling frequencies (i.e., $f_s=100-500$ kHz), whilst higher sampling frequencies enable the use of test signals weaker than the ambient noise (i.e., $SNR \geq -5$ dB). The same holds when comparing the linear chirp to the white noise. Although white noise provides a slighter advantage in terms of estimation error at lower sampling frequencies, the linear chirp performs better at higher sampling frequencies, where it can sustain 5 dB higher ambient noise SPLs.

Therefore, when considering the setup of an experimental acoustic pyrometer, the choice between the two test signals should be made according to the hardware availability or economic considerations.

4. CONCLUSIONS

Acoustic pyrometry is a non-invasive technique for temperature measurement that is gaining more and more interest in turbomachinery. Despite its multiple advantages, several factors may affect the temperature measurement due to a poor TOF estimation of the acoustic signal propagating through the gas exhaust.

In this study, various acoustic sources were investigated for time-of-flight measurements. Estimation error maps were generated to understand which test signal performed better given a particular source and ambient noise SPL and sampling frequency. It was found that linear chirp and white noise provide better TOF estimates along the considered cases. In particular, white noise is preferable at low sampling frequencies in the case of SPLs greater or equal to the ambient noise ones. Conversely, linear chirp is most suited at higher

frequencies, where it provides a slight advantage in signal-to-noise ratio.

Sound), MATLAB Central File Exchange.
Retrieved August 18, 2022.”

5. REFERENCES

- [1] Green, S. F., 1985, “An Acoustic Technique for Rapid Temperature Distribution Measurement,” *J. Acoust. Soc. Am.*, **77**(2), pp. 759–763.
- [2] Bramanti, M., Salerno, E. A., Tonazzini, A., Pasini, S., and Gray, A., 1996, “An Acoustic Pyrometer System for Tomographic Thermal Imaging in Power Plant Boilers,” *IEEE Trans. Instrum. Meas.*, **45**(1), pp. 159–167.
- [3] Kong, Q., Jiang, G., Liu, Y., and Sun, J., 2020, “3D High-Quality Temperature-Field Reconstruction Method in Furnace Based on Acoustic Tomography,” *Appl. Therm. Eng.*, **179**, p. 115693.
- [4] Kleppe, J., Sanchez, J., and Fralick, G., 1998, “The Application of Acoustic Pyrometry to Gas Turbines and Jet Engines,” *34th AIAA/ASME/SAE/ASEE Joint Propulsion Conference and Exhibit*, American Institute of Aeronautics and Astronautics, Cleveland, OH, U.S.A.
- [5] Kleppe, J., Norris, W., McPherson, D., and Fralick, G., 2005, “The Measurement of Performance of Combustors Using Passive Acoustic Methods: Additional Results,” *43rd AIAA Aerospace Sciences Meeting and Exhibit*, American Institute of Aeronautics and Astronautics, Reno, Nevada.
- [6] DeSilva, U., Bunce, R. H., and Claussen, H., 2013, “DRAFT: NOVEL GAS TURBINE EXHAUST TEMPERATURE MEASUREMENT SYSTEM,” p. 7.
- [7] DeSilva, U., Bunce, R. H., Schmitt, J. M., and Claussen, H., 2015, “Gas Turbine Exhaust Temperature Measurement Approach Using Time-Frequency Controlled Sources,” *Volume 6: Ceramics; Controls, Diagnostics and Instrumentation; Education; Manufacturing Materials and Metallurgy; Honors and Awards*, American Society of Mechanical Engineers, Montreal, Quebec, Canada, p. V006T05A001.
- [8] Otero, R., Lowe, K. T., Ng, W. F., and Silas, K. A., 2019, “Coupled Velocity and Temperature Acoustic Tomography in Heated High Subsonic Mach Number Flows,” *Meas. Sci. Technol.*, **30**(10), p. 105901.
- [9] Caposciutti, G., and Ferrari, L., 2021, “Measurement of GT Exhaust Gas Temperature by Acoustic Pyrometry: Preliminary Error Investigation,” *E3S Web Conf.*, **312**, p. 11011.
- [10] Ferrari, L., Caposciutti, G., Pasini, G., Frate, G. F., and Desideri, U., 2022, “Influence of Emitter-Receiver Number on Measurement Accuracy in Acoustic Pyrometry,” *E3S Web Conf.*, **345**, p. 01008.
- [11] Caposciutti, G., and Ferrari, L., 2022, “Acoustic Pyrometry Robustness to Time-of-Flight Estimation Errors,” *J. Eng. Gas Turbines Power*, **144**(2), p. 021015.
- [12] Burnside, N. J., “Atmospheric Attenuation of Sound ([https://www.mathworks.com/matlabcentral/fileexchange/6000-Atmospheric-Attenuation-of-](https://www.mathworks.com/matlabcentral/fileexchange/6000-Atmospheric-Attenuation-of-Sound)